A polarization scheme that resolves cross-peaks with transient absorption and eliminates diagonal peaks in 2D spectroscopy

Kieran M. Farrell[a], Nan Yang[a], and Martin T. Zanni[a,1]

[a]Department of Chemistry, University of Wisconsin–Madison, Madison, WI 53706

Edited by Gregory Engel, Department of Chemistry, Institute for Biophysical Dynamics, and The James Franck Institute, The University of Chicago, Chicago, IL; received September 21, 2021; accepted December 16, 2021 by Editorial Board Member Shaul Mukamel

Two-dimensional (2D) optical spectroscopy contains cross-peaks that are helpful features for determining molecular structure and monitoring energy transfer, but they can be difficult to resolve from the much more intense diagonal peaks. Transient absorption (TA) spectra contain transitions similar to cross-peaks in 2D spectroscopy, but in most cases they are obscured by the bleach and stimulated emission peaks. We report a polarization scheme, $<0°,0°,+\theta_2(t_2),-\theta_2(t_2)>$, that can be easily implemented in the pump-probe beam geometry, used most frequently in 2D and TA spectroscopy. This scheme removes the diagonal peaks in 2D spectroscopies and the intense bleach/stimulated emission peaks in TA spectroscopies, thereby resolving the cross-peak features. At zero pump-probe delay, $\theta_2 = 60°$ destructively interferes two Feynman paths, eliminating all signals generated by field interactions with four parallel transition dipoles, and the intense diagonal and bleach/stimulated emission peaks. At later delay times, $\theta_2(t_2)$ is adjusted to compensate for anisotropy caused by rotational diffusion. When implemented with TA spectroscopy or microscopy, the pump-probe spectrum is dominated by the cross-peak features. The local oscillator is also attenuated, which enhances the signal two times. This overlooked polarization scheme reduces spectral congestion by eliminating diagonal peaks in 2D spectra and enables TA spectroscopy to measure similar information given by cross-peaks in 2D spectroscopy.

cross-peaks | transient absorption | polarization selective 2D IR

Transient absorption (TA) spectroscopy and microscopy are ubiquitously used for measuring kinetics in chemical, biological, and material sciences. TA spectroscopy initiates excited-state dynamics with a pump pulse and tracks their evolution with a probe pulse, yielding kinetic information. The polarization of the pump and probe fields strongly affects the utility and interpretation of TA data (1–5). The choice of pulse polarization can be employed to ease interpretation or extract particular information. For example, under three-dimensional (3D) isotropic conditions, kinetics measured at 54.7° relative angle (magic angle) between pump and probe polarizations are insensitive to molecular rotation (6–11). Alternatively, the anisotropy can be calculated after independently measuring parallel and perpendicularly polarized pulses, giving a signal that depends on rotational diffusion and not population relaxation (6–11). Magic angle and anisotropy measurements are textbook experiments.

A technique closely related to TA spectroscopy is two-dimensional (2D) spectroscopy, such as 2D infrared (IR) and 2D electronic spectroscopy. TA and 2D spectroscopies are alike in that they both measure a signal created by three electric field interactions from the pulse sequence, which makes them third-order nonlinear techniques (3, 12, 13). Because TA and 2D spectroscopy are both third-order techniques, the polarization dependence of their spectra is identical. However, the way in which the experiments are implemented puts physical limitations on the polarizations that can be applied. For TA spectroscopy, the first two interactions (E_1 and E_2) are created by the pump pulse and third by the probe pulse (E_3), followed by the emitted field (E_{emit}) that ultimately becomes the signal. For time-domain 2D spectroscopy, there are also three interactions, one each from two separate pump pulses (E_1 and E_2) and the third from the probe pulse (E_3), followed by E_{emit}. The signals of both experiments depend on the orientational average of four electric fields with the sample, which is often written as the four-point orientational average $<E_1,E_2,E_3,E_{emit}>$.

Since TA spectroscopy only uses two laser pulses, polarization control is traditionally limited to the relative angle between pump and probe polarizations. When 2D spectroscopy was first developed, it was implemented in a four-wave mixing geometry that allowed all three pulse polarizations to be individually set along with the polarization of the emitted field (14–16). This new capability led to the derivation of the full fourth-order orientational correlation function (4, 10, 17) and more advanced polarization schemes that determined the angle between coupled oscillators (17), suppressed peaks (18), and enhanced signal-to-noise (19, 20). One of the most unique polarization schemes was $<E_1,E_2,E_3,E_{emit}> = <-45°,+45°,90°,0°>$, with the angles defined in the laboratory-fixed frame. This polarization scheme eliminates the diagonal peaks from the 2D spectrum under 3D isotropic conditions, isolating the desired cross-peak features (18). This method works by destructively interfering the $<0°,90°,0°,90°>$ and the $<0°,90°,90°,0°>$ signals in situ. In the same publication, Hochstrasser and coworkers proposed $<-60°,+60°,0°,0°>$, which

Significance

Observation of cross-peaks is one of the hallmark advantages of multidimensional spectroscopy. Often times, cross-peaks overlap with strong diagonal peak features, obfuscating information that is useful for determining molecular structure. Here, we present a polarization scheme that eliminates diagonal peaks, revealing the weaker cross-peak features. This polarization scheme can be applied to one-dimensional transient absorption spectroscopy. As a result, transient absorption spectroscopy can now access information that previously required two-dimensional spectroscopies.

Author contributions: K.M.F. and M.T.Z. designed research; K.M.F. and N.Y. performed research; K.M.F. analyzed data; and K.M.F. and M.T.Z. wrote the paper.

Competing interest statement: M.T.Z. is a co-owner of PhaseTech Spectroscopy, Inc., which sells 2D IR/visible spectrometers, pulse shapers, and high-repetition rate MCT detection electronics.

This article is a PNAS Direct Submission. G.E. is a guest editor invited by the Editorial Board.

[1]To whom correspondence may be addressed. Email: zanni@chem.wisc.edu.

This article contains supporting information online at http://www.pnas.org/lookup/suppl/doi:10.1073/pnas.2117398119/-/DCSupplemental.

Published February 3, 2022.

removes diagonal peaks but does not compensate for rotational diffusion (18, 21). Ginsberg et al. and Read et al. implemented <−60°,+60°,0°,0°> in the visible (22, 23). One can independently measure and subtract spectra collected for each of these polarizations (24), but subtraction afterward is usually less accurate and sometimes very difficult, such as when measuring the kinetics of protein aggregation. Besides polarization schemes, peaks can be removed by fitting or by isolating interstate coherences (25–27).

Diagonal peak suppression was widely implemented in 2D spectroscopy (18, 22, 23, 28–38) until pump-probe beam geometries began replacing the four-wave mixing geometry. The most common pump-probe implementation of 2D spectroscopy is using a pulse shaper to create the two pump pulses (39, 40). Pulse-shaping 2D spectroscopy has many advantages over four-wave mixing 2D spectroscopy, such as phase stability, shot-to-shot readout, and absorptive line shapes (41, 42). One drawback has been, like TA spectroscopy, that the pump pulses are collinear and so their polarizations are difficult to control independently (43). As a result, the <−45°,+45°,90°,0°> polarization scheme that was so useful for visualizing cross-peaks is now less utilized. We note that <−45°,+45°,90°,0°> can be implemented in pump-probe 2D spectroscopies that use interferometers (44–46), birefringent wedges (37, 47), and polarization pulse shapers (43).

In this paper we report a polarization scheme that can be implemented in the pump-probe geometry used by 2D and TA spectroscopies. Spectra collected in this polarization scheme only contain features from nonparallel transition dipoles. For 2D spectroscopy, this scheme eliminates the diagonal peaks so that only cross-peaks remain in the spectra. For TA spectroscopy, this scheme means that TA spectra provide the same information as the cross-peaks in 2D spectra, as we demonstrate. The polarization scheme we implement is <0°,0°,+60°,−60°>, or more generally, <0°,0°,+$\theta_2(t_2)$,−$\theta_2(t_2)$> [where $\theta_2(t_2)$ depends on the pump-probe delay, t_2]. Permutational symmetry holds for the fourth-rank orientational response at $t_2 = 0$ and so <0°,0°,+60°,−60°> gives an equivalent 2D spectrum to <−60°,+60°,0°,0°>. What has been overlooked is that <0°,0°,+60°,−60°> can be experimentally implemented in the pump-probe geometry by adding two polarizers in the probe beam (*SI Appendix*, Fig. S1), whereas <−60°,+60°,0°,0°> cannot. As a result, the <0°,0°,+60°,−60°> polarization allows TA spectroscopy to obtain coupling information that, until now, could only be resolved by 2D spectroscopy. The method promises to revive 2D spectra of cross-peaks, enable TA spectroscopy to measure couplings, and permit new experiments like TA imaging of coupled modes. In what follows, we first qualitatively describe the method and experimentally demonstrate it then present the theoretical underpinnings and discussion of its strengths, weaknesses, and potential uses.

Experimental Demonstration

Prior to delving into the theoretical formalism, we provide a simple example to illustrate the utility of this pulse sequence for 2D and TA spectroscopies. The <0°,0°,+60°,−60°> polarization scheme is demonstrated using (acetylacetonato)dicarbonyl iridium(I) (IDC) dissolved in hexane. IDC is a model compound often used to test 2D IR pulse sequences (48). It consists of two carbonyl groups coordinated to an iridium metal center at a 90° angle relative to each other. The two carbonyl local modes are strongly coupled and delocalize to yield symmetric and antisymmetric stretching modes at 2,076 cm^{-1} and 2,002 cm^{-1}, respectively. The transition dipoles for these two modes are orthogonal. Fig. 1*A* shows the 2D IR spectrum of IDC in hexane for the <0°,0°,0°,0°> polarization with the delay between the pump pulses and the probe pulse set to $t_2 = 0$. The 2D IR spectrum consists of four pairs of peaks: two pairs on the diagonal at the fundamental frequencies, which we refer to as "diagonal peaks," and two sets off-diagonal peaks that correlate the two fundamental frequencies, which we refer to as "cross-peaks." The diagonal peak pairs are separated by the diagonal anharmonicity, Δ_{ii}, while the cross-peak spacing gives

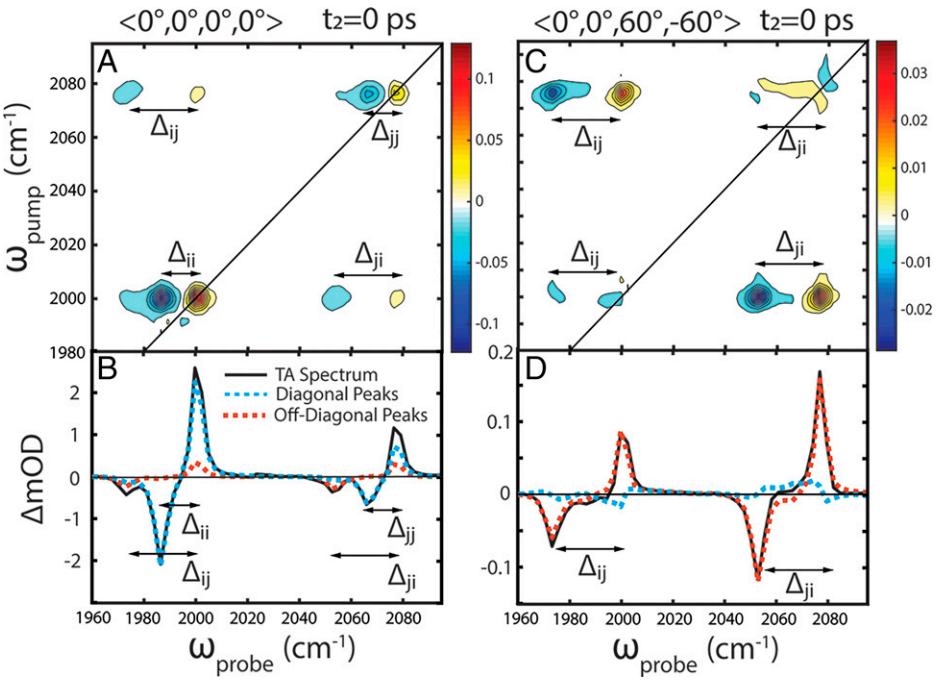

Fig. 1. Spectra showing the removal of diagonal peaks using <0°,0°,+60°,−60°>. Two-dimensional IR spectrum of IDC at $t_2 = 0$ ps for (*A*) <0°,0°,0°,0°> and (*C*) <0°,0°,60°,−60°> polarization schemes. (*B* and *D*) Black: TA spectra corresponding to the 2D spectra in *A* and *C*, respectively. Blue: exclusive projection of the diagonal quadrants of the 2D spectrum onto the probe axis, mathematically equivalent to a TA spectrum of on-diagonal peaks. Red: exclusive projection of off-diagonal quadrants, equivalent to a TA spectrum of off-diagonal cross-peaks.

the off-diagonal anharmonicity, Δ_{ij}, which are 14 cm^{-1} and 27 cm^{-1}, respectively. The spectra use an absorptive pulse sequence, meaning that they contain both rephasing and nonrephasing spectra; the nonrephasing spectra also have cross-peaks on the diagonal, although they are much weaker than the larger diagonal peaks.

Shown in Fig. 1*B* (solid, black) is the TA spectrum of the same sample collected in <0°,0°,0°,0°> with a pump-probe delay of $t_2 = 0$. One reason that IDC is used as a model compound is because Δ_{ij} is larger than Δ_{ii} and the linewidths are narrow such that transitions that create cross-peaks in a 2D IR spectrum can be resolved in the TA spectrum. These peaks are labeled with Δ_{ii} and Δ_{ij}. If one can measure Δ_{ii} and Δ_{ij} from a TA spectrum, then 2D IR spectroscopy is not necessary to determine the couplings. Typically, these transitions cannot be identified because the TA spectra are too congested and obscured by the diagonal peaks.

In addition to the TA spectrum, the projections of the 2D spectrum onto the probe axis are also shown. Projections are calculated by integrating over the pump axis and are mathematically equivalent to a TA spectrum. The projection across the entire 2D spectrum reproduces the TA spectrum (*SI Appendix*, Fig. S5). Shown in Fig. 1*B* is the projection of just the diagonal peaks (blue, dashed) and just the cross-peaks (red, dashed), calculated by integrating exclusively over diagonal and off-diagonal quadrants of the 2D spectrum, respectively. The TA spectrum is largely reproduced by the diagonal projection, but it still contains some contribution from the off-diagonal projection. Thus, the TA spectrum contains both diagonal and cross-peaks but is dominated by the much larger diagonal peaks.

Fig. 1 *C* and *D* shows the 2D IR and TA spectrum of IDC collected in <0°,0°,+60°,−60°>, which is done by placing two polarizers into the probe beam: one before the sample and the other after. The diagonal peaks are strongly suppressed, and the cross-peaks are the dominant features. Diagonal peaks are suppressed 77 times and the cross-peaks are 1.2 times larger relative to <0°,0°,0°,0°>. There are also weak on-diagonal cross-peaks that contain the same coupling information as the off-diagonal cross-peaks but have a different orientational response and lineshape. Also shown are projections of the diagonal and off-diagonal quadrants of the 2D IR spectrum. The TA spectrum no longer contains the diagonal peaks, making the transitions that create the cross-peaks the dominant features. Δ_{ij}, and hence the couplings, are now easily determined from the TA spectrum. Thus, the <0°,0°,+60°,−60°> polarization scheme expands the power of TA spectroscopy, making it possible to obtain the same cross-peak information that was previously best resolved by a 2D measurement.

The <0°,0°,+60°,−60°> polarization scheme eliminates the diagonal peaks at $t_2 = 0$ in the limit of infinitely short laser pulses. It will also eliminate the diagonal peaks for later time delays if the molecules do not rotate. If orientational relaxation occurs, then the diagonal peaks grow in on the timescale of the anisotropy decay. Nonetheless, the diagonal peaks can be eliminated for $t_2 > 0$ by using <0°,0°,$\theta_2(t_2)$,−$\theta_2(t_2)$> where $\theta_2(t_2)$ is calculated from the rotational diffusion constant. The theory behind these claims and evaluation of $\theta_2(t_2)$ is given in *Theory*, following the experimental demonstration here.

Fig. 2 *A* and *B* shows the 2D IR and TA spectra of IDC for <0°,0°,+60°,−60°> at a pump-probe delay of $t_2 = 6$ ps. Diagonal peaks are now present in the 2D spectra as are new cross-peaks at (ω_{pump}, ω_{probe}) = (2,076, 1,986) cm^{-1} and (2,002, 2,066) cm^{-1}. Khalil et al. showed that the new peaks arise from population transfer, which is why they are offset by Δ_{ii} (49). To remove the diagonal peaks, we set the polarization to <0°,0°,54.1°,−54.1°>, as shown in Fig. 2 *C* and *D*. Diagonal peaks are now absent from the 2D spectrum and TA spectra are almost identical to the projection of the cross-peaks. Notice that the off-diagonal cross-peaks created by population relaxation remain but not the diagonal peaks. This fact is explained in *Theory*. The diagonal peaks can be removed for any time delay. Fig. 2*E* plots the intensity of the lower diagonal peak (2,002, 1,988) cm^{-1} for the fixed angles <0°,0°, +60°,−60°> (red). It is small at $t_2 = 0$ and grows in intensity due to rotational diffusion. Shown in black is the intensity of the same peak for <0°,0°,$\theta_2(t_2)$,−$\theta_2(t_2)$>, in which the angles are set at each time delay according to Eq. **9** given below. The intensity is now close to zero at each delay because the diagonal peaks are suppressed. Thus, with the proper choice of angles, the diagonal peaks can be removed from the 2D and the TA spectra for any given waiting time, allowing the evolution of couplings to be observed. In *Discussion* we consider limits and caveats to this general statement.

The general utility of this polarization scheme is demonstrated in Fig. 3 with spectra collected on a thin section of human tissue taken from an eye lens. The 2D IR spectrum shown in Fig. 3*A* is representative of spectra used to assess cataract formation via the weak β-sheet cross-peak labeled with an asterisk. This spectrum is collected with <90°,90°,0°,0°> and the diagonal peaks are the dominant figures. Fig. 3*B* is a spectrum collected in <0°,0°,60°,−60°> at $t_2 = 0$. The diagonal peaks are suppressed 88 times, so that the previously utilized cross-peak is now the dominant feature and many additional cross-peaks are revealed. Previously obscured cross-peaks are now visible, which may be created by couplings between α-helical and β-sheet structures in the crystallin proteins. Our prior report on cataracts correlated amyloid β-sheet structures to light scattering (50). These new features might enable one to correlate amorphous aggregates with light scattering, which is another possible source for the disease. These spectra are representative of what might be expected for inhomogeneously broadened and congested spectra.

Theory

In this section we present the theoretical formalism behind the proposed polarization scheme. We explain why the diagonal peaks are removed, present a generalized formula for how to calculate $\theta_2(t_2)$, and calculate the enhancement in signal strength due to the attenuation of the probe beam. We also refer readers to Chapter 5 of Hamm and Zanni for background reading (5).

Diagonal Peak Removal Using <0°,0°,+60°,−60°>. We begin by describing the orientational response of the <0°,0°,+60°,−60°> signal under 3D isotropic conditions and show how it removes diagonal peaks, thus isolating cross-peaks. Polarization schemes can be decomposed into linear combinations of the four isotropic symmetry allowed polarizations: XXXX, YYXX, XYXY, and XYYX, where X and Y are orthogonal polarizations in the laboratory frame. The four-wave mixing orientational correlation functions for each of these polarizations have been evaluated for the eight Liouville pathways contributing to the 2D IR spectrum. Their derivation can be found elsewhere (4, 5). These functions scale the intensity of the peaks in 2D and TA spectra. The orientational correlation function for the *iiii* pathway is the scaling factor for the diagonal peaks because all four electric field interactions occur with the same oscillator. The other three pathways (*iijj*, *ijij*, and *ijji*) are for the cross-peaks.

Eq. **1** shows the decomposition of <0°,0°,+θ,−θ> into two of the four symmetry-allowed polarizations:

$$\begin{aligned}\langle 0^\circ, 0^\circ, +\theta, -\theta\rangle &= XX[\cos(\theta)X \\ &\quad +\sin(\theta)Y][\cos(-\theta)X + \sin(-\theta)Y] \qquad \textbf{[1a]}\\ &= \left(\cos^2(\theta)XXXX + \sin\theta\cos\theta XXYX\right. \\ &\quad \left. -\sin\theta\cos\theta XXXY - \sin^2(\theta)XXYY\right) \qquad \textbf{[1b]}\end{aligned}$$

CHEMISTRY

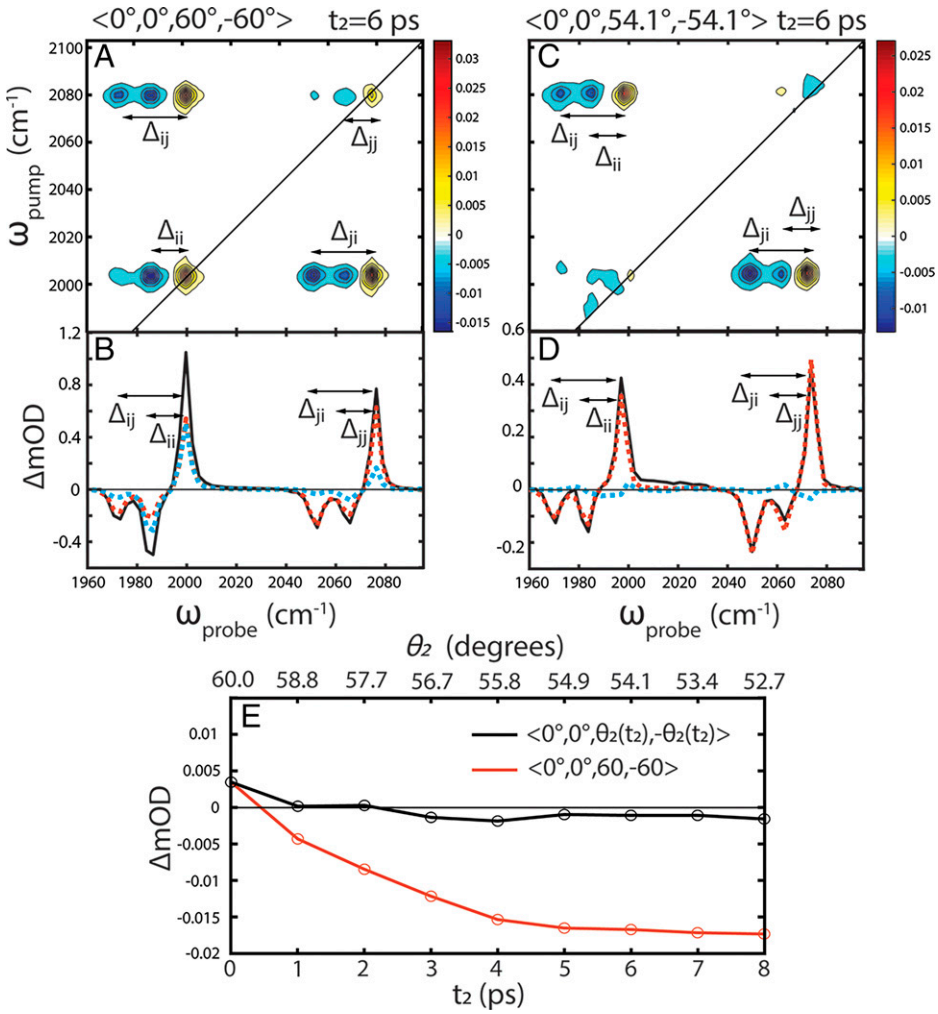

Fig. 2. Removal of diagonal peaks at later waiting times using <0°,0°,$\theta_2(t_2)$,$-\theta_2(t_2)$>. (*A* and *C*) Two-dimensional IR spectrum of IDC collected in <0°,0°,+60°,−60°> and <0°,0°,+54.1°,−54.1°> at a 6-ps pump-probe delay. (*B* and *D*) Black, solid: TA spectrum, (red, dashed) cross-peak projection, and (blue, dashed) diagonal peak projection for spectra collected in <0°,0°,+60°,−60°> and <0°,0°,54.1°,54.1°> at a 6-ps pump-probe delay. (*E*) Intensity of diagonal peak at (2,002, 1,988) cm^{-1} in the 2D spectrum for <0°,0°,+60°,−60°> (red) and <0°,0°,$\theta_2(t_2)$,$-\theta_2(t_2)$> (black) as a function of pump-probe delay.

$$= \left(\cos^2(\theta)XXXX - \sin^2(\theta)XXYY\right) \quad \textbf{[1c]}$$

$$\langle 0°, 0°, +60°, -60° \rangle = \frac{1}{4}(XXXX - 3XXYY). \quad \textbf{[1d]}$$

Eq. **1c** is reached by the fact that the orientational average of the XXYX and XXXY polarizations go to zero for all dipole-allowed Liouville pathways under isotropic conditions (51). The isotropic orientational correlation function at $t_2 = 0$ for a pathway that gives a diagonal peak (*iiii*) is 1/5 and 1/15 for XXXX and XXYY, respectively. As a result, the diagonal peaks are three times more intense when measured with XXXX than with XXYY polarizations. By setting $\theta = 60°$, the XXXX and XXYY pathways are scaled such that diagonal peaks are equal in magnitude and opposite in sign. Therefore, diagonal peaks from XXXX and XXYY destructively interfere and are removed. The cross-peaks intensities depend on the choice of polarization and relative oscillator angle, $\theta_{\alpha\beta}$. Cross-peaks are not removed if the coupled transition dipoles are nonparallel. XXXX and XXYY can also be measured separately and manually subtracted to obtain the cross-peaks, as we experimentally demonstrate in *SI Appendix*.

Generalized Formula for Diagonal Peak Removal. There exist other polarization conditions which are both compatible with a pulse shaper and remove diagonal peaks. To find them, we evaluate the orientational correlation function for the *iiii* pathway using the formalism developed by Hochstrasser, keeping the angle for the first two fields the same (4):

$$\left\langle \left(\hat{\mu}_\alpha \cdot \hat{E}_1\right)\left(\hat{\mu}_\alpha \cdot \hat{E}_1\right)\left(\hat{\mu}_\alpha \cdot \hat{E}_2\right)\left(\hat{\mu}_\alpha \cdot \hat{E}_3\right)\right\rangle$$

$$= \frac{1}{30}\begin{pmatrix} \cos(\theta_{23}) \\ \cos(\theta_{12})\ \cos(\theta_{13}) \\ \cos(\theta_{13})\ \cos(\theta_{12}) \end{pmatrix}^T \begin{pmatrix} 4 & -1 & -1 \\ -1 & 4 & -1 \\ -1 & -1 & 4 \end{pmatrix} \begin{pmatrix} \cos(\theta_{\alpha\beta})\ \cos(\theta_{\gamma\delta}) \\ \cos(\theta_{\alpha\gamma})\ \cos(\theta_{\beta\delta}) \\ \cos(\theta_{\alpha\delta})\ \cos(\theta_{\beta\gamma}) \end{pmatrix}. \quad \textbf{[2]}$$

In Eq. **2**, μ_α is the molecular transition dipole vector for dipole α and 1, 2, and 3 index the pump, probe, and local oscillator (LO) fields, respectively. *SI Appendix*, Fig. S2*A* shows the orientational function of the diagonal peak for <0°,0°,θ_2,θ_3> with $\theta_{\alpha\beta} = 90°$. *SI Appendix*, Fig. S2 *B* and *C* plot the orientational correlation function for the cross-peaks. Black lines in *SI Appendix*, Fig. S2 are drawn for polarizations in which diagonal peaks are removed, of which there are many. The cross-peaks also depend on the choice of angles. When calculating a spectrum on a linear scale, <0°,0°,+60°,−60°> and <0°,0°, +120°, +60°> provide the largest cross-peak intensities.

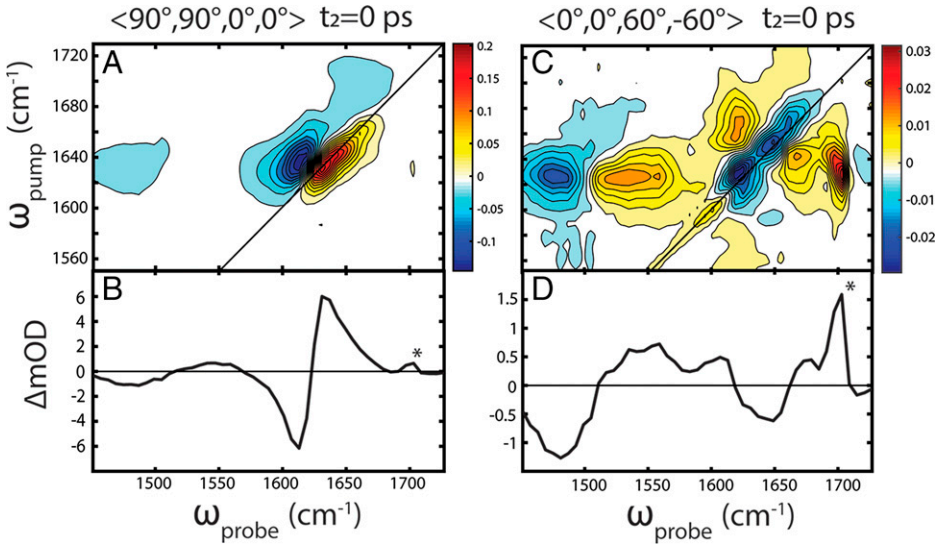

Fig. 3. Removal of diagonal peaks from a spectrum of a human eye lens cross section. (*A*) Two-dimensional IR spectrum the amide I vibration measured in <90°,90°,0°,0°>. (*B*) Scaled projection of <90°,90°,0°,0°> 2D spectrum onto the probe axis, corresponding to the TA spectrum. (*C*) Two-dimensional IR spectrum the amide I vibration measured in <0°,0°,+60°,−60°>. (*D*) Scaled projection of <0°,0°,+60°,−60°> 2D spectrum onto the probe axis.

Signal-to-Noise Enhancement from an Attenuated Local Oscillator. Two-dimensional and TA spectroscopy are heterodyne-detected, meaning that the interference term between E_3 and E_{emit} is measured. Thus, data are calculated as a differential optical density:

$$-\Delta OD = \log\left(\frac{\text{pump on}}{\text{pump off}}\right) = \log\left(\frac{E_3^2 + E_{\text{emit}}^2 + 2E_3E_{\text{emit}}}{E_3^2}\right) \approx \frac{2E_{\text{emit}}}{E_3}. \quad [3]$$

It is evident from Eq. **3** that reducing the intensity of the probe on the detector without reducing the intensity of the emitted field would enhance the measured ΔOD, a fact that has been utilized in a number of scenarios (19, 20, 45, 52, 53).

After the sample, E_3 passes through the same polarizer as E_{emit}, which projects E_3 onto E_{emit}. E_3 does not have the same polarization as E_{emit} for angles that remove diagonal peaks. As a result, E_3 will be attenuated and the ΔOD will be enhanced. To calculate the expected enhancement, we note that E_3 is attenuated according to Eq. **4**:

$$E_3 \propto \cos(\theta_3 - \theta_2). \quad [4]$$

Inserting Eqs. **2** and **4** into Eq. **3**, we obtain the enhanced ΔOD:

$$-\Delta OD \propto \frac{\langle(\hat{\mu}_\alpha \cdot \hat{E}_1)(\hat{\mu}_\beta \cdot \hat{E}_1)(\hat{\mu}_\gamma \cdot \hat{E}_2)(\hat{\mu}_\delta \cdot \hat{E}_3)\rangle}{\cos(\theta_3 - \theta_2)}. \quad [5]$$

For <0°,0°,+60°,−60°>, Eq. **5** gives a 2× enhancement of signal. *SI Appendix*, Fig. S3 contains plots of the enhancement as a function of θ_2 and θ_3. It happens that LO attenuation enhances cross-peaks to a common value for all polarizations that remove diagonal peaks. Therefore, in the limit of no noise, all angles that remove diagonal peaks should perform equally well. In practice, one needs sufficient E_3 intensity to be measured on the detector. Experimental evidence for the 2× enhancement is provided in *SI Appendix* (*SI Appendix*, Figs. S6 and S7).

Effect of Rotational Diffusion on Diagonal Peak Removal. The theoretical description above only applies to $t_2 = 0$ because the orientational functions depend on the pump-probe delay (54). The orientational correlation functions under 3D isotropic conditions for the *iiii* pathways including rotational diffusion during the pump-probe delay are shown in Eq. **6a–d** (4, 5):

$$\langle X_iX_iX_iX_i\rangle = \frac{1}{45}\left[4e^{-6Dt_2} + 5\right] \quad [6a]$$

$$\langle X_iX_iY_iY_i\rangle = \frac{1}{45}\left[5 - 2e^{-6Dt_2}\right] \quad [6b]$$

$$\langle X_iY_iX_iY_i\rangle = \frac{1}{15}e^{-6Dt_2} \quad [6c]$$

$$\langle X_iY_iY_iX_i\rangle = \frac{1}{15}e^{-6Dt_2}. \quad [6d]$$

In Eq. **6**, D is the rotational diffusion constant. Evaluating Eq. **6** at $t_2 = 0$ yields a 3:1 ratio between XXXX and XXYY. For $t_2 > 0$, XXXX and XXYY no longer have a ratio of 3:1 for the diagonal peaks. Therefore, they no longer cancel for <0°,0°, +60°,−60°>. As a result, if the polarizations are held at <0°,0°,+60°,−60°> and the pump-probe delay is increased, the diagonal peaks reappear in the spectrum.

In general, diagonal peaks will be removed when the following condition is satisfied:

$$a\langle X_iX_iX_iX_i\rangle = -(b\langle X_iX_iY_iY_i\rangle + c\langle X_iY_iX_iY_i\rangle + d\langle X_iY_iY_iX_i\rangle). \quad [7]$$

In Eq. **7**, a, b, c, and d are the projection of XXXX, XXYY, XYXY, and XYYX onto θ_3 for the polarization scheme <θ1,θ1,θ2,θ3>:

$$a = \cos^2\theta_1 \cos\theta_2 \cos\theta_3 \quad [8a]$$

$$b = \cos^2\theta_1 \sin\theta_2 \sin\theta_3 \quad [8b]$$

$$c = \cos\theta_1 \sin\theta_1 \cos\theta_2 \sin\theta_3 \quad [8c]$$

$$d = \cos\theta_1 \sin\theta_1 \sin\theta_2 \cos\theta_3. \quad [8d]$$

Inserting Eqs. **6** and **8** into Eq. **7**, setting $\theta_1 = 0$, constraining θ_3 such that $\theta_3 = -\theta_2$, and solving for θ_2 yields

$$\theta_2 = \tan^{-1}\left(\sqrt{\frac{4e^{-6Dt_2} + 5}{5 - 2e^{-6Dt_2}}}\right). \quad [9]$$

Thus, the polarizations of E_3 and E_{emit} can be tuned as a function of t_2 and D to satisfy Eq. **7** and remove the diagonal peaks. Just as there are many ways to remove diagonal peaks at $t_2 = 0$, Eq. **9** is just one of many conditions in which rotational effects can be compensated for $t_2 > 0$. For example, Eq. **7** can be solved for θ_3 as a function of t_2, D and a fixed θ_2. The only

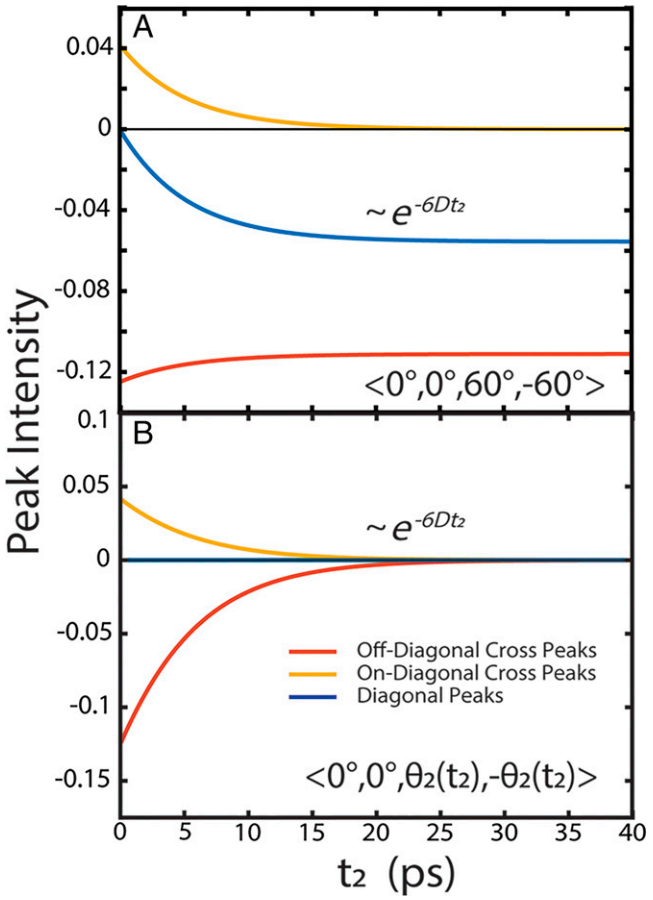

Fig. 4. Waiting time dynamics of <0°,0°,+60°,−60°>. Diagonal peak (blue), off-diagonal cross-peak (red), and on-diagonal cross-peak (yellow) intensities calculated from the orientational correlation functions in Eq. **7**. (*A*) Relative peak intensities for <0°,0°,+60°,−60°>. (*B*) Relative peak intensities for <0°,0°,$\theta_2(t_2)$,$-\theta_2(t_2)$>.

unknown is the rotational diffusion coefficient, which can be obtained from an anisotropy measurement.

Fig. 4 *A* and *B* simulates the cross-peak intensity as a function of t_2 for <0°,0°,+60°,−60°> and <0°,0°,+$\theta_2(t_2)$,−$\theta_2(t_2)$>, respectively, where $\theta_2(t_2)$ is the polarization angle given by Eq. **9**. The diffusion coefficient in this simulation was 0.035 ps^{-1}. Simulations details are included in *SI Appendix*. Fig. 4*A* shows that diagonal peaks reappear with pump-probe delay for <0°,0°,+60°,−60°>, ultimately reaching an offset. On the other hand, <0°,0°,+$\theta_2(t_2)$,−$\theta_2(t_2)$> eliminates diagonal peaks at all waiting times, when $\theta_2(t_2)$ is adjusted for each delay. Fits of cross-peak intensities in Fig. 4*B* indicate that they decay with the rotational anisotropy (i.e., with a rate of 6D). Likewise, diagonal peaks in Fig. 4*A* reappear with rate of 6D. Thus, <0°,0°,+$\theta_2(t_2)$,−$\theta_2(t_2)$> removes diagonal peaks and preserves cross-peaks prior to anisotropy decay. We refer to orientational relaxation and anisotropy decay interchangeably. Mechanical rotations, which are one mechanism of orientational relaxation, are referred to as rotational diffusion.

We note that the simulated peak intensities are opposite in sign compared to experimental data in Fig. 1. This sign flip is due to the projection of the probe onto −60° by the polarizer after the sample (*SI Appendix*). In this simulation, the relative oscillator angle was set to 90°. Reappearance of cross-peaks at <0°,0°,+60°,−60°> and decay of signal at <0°,0°,+$\theta_2(t_2)$, −$\theta_2(t_2)$> occurs with a rate of 6D regardless of the relative angle. The intensity and sign of the cross-peaks depends on the relative angles. Simulations for other relative angles are shown in *SI Appendix*, Fig. S4.

Discussion and Additional Data

Experiments and theory presented above illustrate the utility of this polarized pulse sequence in 2D and TA spectroscopy. We now discuss some of the more nuanced aspects of these experiments. For background reading on the topics below, please see Chapter 4 of Hamm and Zanni (5).

On-Diagonal Cross-Peaks and Rephasing/Nonrephasing Spectra. Most discussion of cross-peaks to this point has focused on the off-diagonal cross-peaks. Some Feynman pathways lead to cross-peaks that appear along the diagonal, shown in Fig. 5*A* (5, 53). The first and last dipole interactions are with *i*, so they spectrally overlap the *iiii* diagonal peaks, but since the fields interact with both transition dipoles *i* and *j*, they are cross-peaks. If *i* is not parallel with *j*, they will appear in the <0°, 0°,+60°,−60°> spectra. The pathways are nonrephasing and therefore have antidiagonal lineshapes. In the impulsive limit at $t_2 = 0$, they should be roughly one-third the intensity of the off-diagonal cross-peaks and opposite in sign in the absorptive spectrum. Due to vibrational dynamics occurring during finite pulse widths, the actual intensity ratio may vary by system. This ratio holds for all $\theta_{\alpha\beta}$ angles. In this spectrum, they appear weaker because of their twisted nonrephasing lineshapes. The TA spectrum for <0°,0°,+$\theta_2(t_2)$,−$\theta_2(t_2)$> will often contain contributions from both the off-diagonal and weaker on-diagonal cross-peaks. There are also cross-peaks created by forbidden pathways, which we do not discuss here (5).

It is possible to generate 2D spectra that do not have any cross-peaks on the diagonal by measuring or calculating the rephasing spectra. All of the spectra shown above are absorptive spectra, meaning that they are a sum of the rephasing and nonrephasing pathways (55). One can separately measure the rephasing and nonrephasing spectra or calculate the respective rephasing and nonrephasing spectra from an absorptive spectrum using a finite frequency Kramers–Kronig inversion (19). Shown in Fig. 5 *B* and *C* are the rephasing and nonrephasing spectra extracted computationally from the absorptive spectrum of Fig. 1*C*. In the rephasing spectrum, there are no on-diagonal cross-peaks. The on-diagonal cross-peaks only appear in the nonrephasing spectrum because they are only generated from nonrephasing Feynman pathways. While absorptive spectra are desirable because of their narrow linewidths and lack of phase twist, there are situations when it may be advantageous to measure or calculate the rephasing and nonrephasing spectra separately to better resolve the cross-peaks (27).

Experimental Validation That Diagonal Peaks Reappear with the Rotational Relaxation Time. We show in this section that the diagonal features reappear when measuring in <0°,0°,+60°, −60°> due to anisotropy decay, such as that caused by rotational diffusion or energy transfer to nonparallel modes. In Fig. 6*A* we compare the intensity of the overtone diagonal peak at (2,002, 1,986) cm^{-1} measured in <0°,0°,+60°,−60°> to the anisotropy decay. Regardless of polarization, peaks still decay due to population relaxation. Thus, to normalize for population relaxation, the kinetic trace of the diagonal peak measured in <0°,0°,+60°,−60°> was divided by a kinetic trace of the same peak measured at magic angle. This trace is shown in Fig. 6*A*. Monoexponential fits reveal that diagonal peaks reappear with a 0.0236 ± 0.0007 ps^{-1} rate. Fits to the anisotropy decay yields a diffusion coefficient of 0.0231 ± 0.0015 ps^{-1} (Fig. 6*A*). These rates are within uncertainty of each other, confirming that orientational relaxation is responsible for the appearance of diagonal peaks in the <0°,0°,+60°,−60°> polarization.

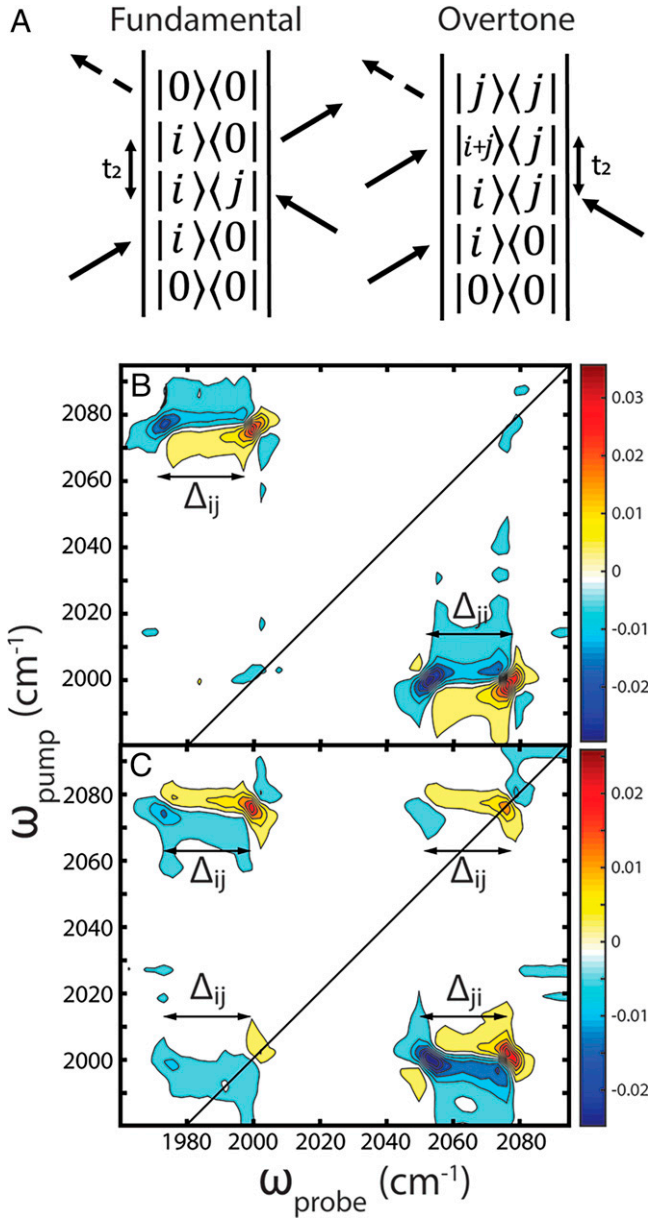

Fig. 5. Isolation of rephasing an nonrephasing spectra. (*A*) Feynman diagrams for the fundamental and overtone on-diagonal cross-peaks. (*B*) Rephasing part of the spectrum collected in <0°,0°,+60°,−60°> at $t_2 = 0$ that is shown in Fig. 1*C*. (*C*) Nonrephasing part of the spectrum collected in <0°,0°,+60°,−60°> at $t_2 = 0$ that is shown in Fig. 1*C*.

In addition to rotations, energy transfer can cause the appearance of diagonal peaks if energy transfer occurs to nonparallel, degenerate modes. Consider the situation in which the two pump fields excite population in the mode *i*, which then undergoes population transfer to a degenerate mode *j*. If *i* and *j* are not parallel, then this peak will appear on the diagonal and appear in <0°,0°,+60°,−60°> spectra. As a result, energy transfer can manifest in the data as orientational relaxation. Energy transfer among degenerate modes commonly occurs in liquids and the excited-state dynamics of conjugated polymers (56, 57). In general, nondegenerate energy transfer gives rise to peaks on the diagonal. If nondegenerate energy transfer is not accompanied by orientational relaxation, then these peaks are removed by <0°,0°,+60°,−60°> because they are *iiii* pathways.

It does not matter whether orientational relaxation is caused by mechanical motions or energy transfer; one can still eliminate the diagonal peaks for monoexponential decay by calculating the required angle using Eq. **9** and orientational diffusion constant. The orientational diffusion constant can be determined, for example, by measuring the anisotropy. The case of multiexponential anisotropy decay is discussed in *Untested Ideas for Future Directions*.

Methods to Obtain the Rotational Diffusion Constant, D, Needed to Remove Diagonal Peaks. The orientational diffusion constant is often determined by measuring the anisotropy decay, calculated by a ratio of signals measured in XXXX and XXYY. That method can be used here. An alternative method that we employed to determine the angles used in Fig. 2 was to set a nonzero pump-probe delay (e.g., $t_2 = 6$ ps) and then scan angles θ_2 and θ_3 ($\theta_2 = -\theta_3$) until the diagonal peaks are removed. Eq. **9** can then be used to back-calculate D. For other time delays, D is then reinserted into Eq. **9** to obtain $\theta_2(t_2)$.

When using broadband pulses, both diagonal and on-diagonal cross-peaks contribute to the spectrum for both 2D and TA spectra. Therefore, in the approach we used for Fig. 2, zero intensity occurs when the diagonal peaks destructively interfere with the on-diagonal cross-peaks in the 2D spectrum. For IDC, the on-diagonal cross-peaks are 43 times smaller than the diagonal peaks at $t_2 = 0$. Thus, diagonal peak reduction is set at 43 times. The reduction would be worse if broadband TA spectroscopy were used to obtain D, because the diagonal signal would interfere with both the on-diagonal and off-diagonal

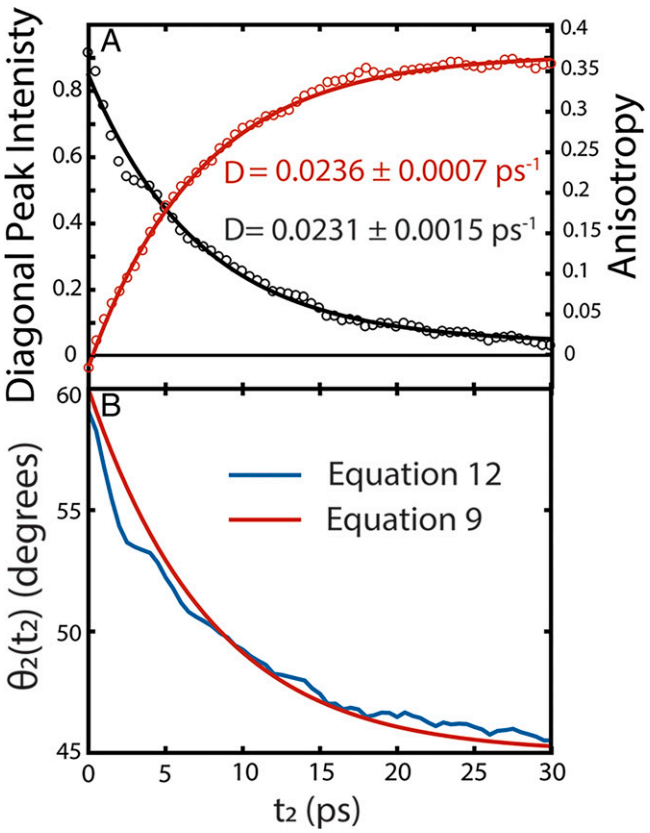

Fig. 6. Analysis of diagonal peak reappearance and calculation of compensation angles. (*A*) Red: trace of diagonal overtone peak at (2,002, 1,986) cm^{-1} measured in <0°,0°,+60°,−60°> divided by a trace of the same peak measured at the magic angle. Black: anisotropy decay of the diagonal overtone peak at (2,002, 1,986) cm^{-1} obtained from the 2D IR spectra. Uncertainties are within 95% confidence. (*B*) The angle required to remove diagonal peaks a later waiting times calculated using Eq. **12** (blue) and Eq. **9** (red).

cross-peaks. If better accuracy is required, one can perform this method with a narrowband pump. If diagonal peaks are resolved, then the narrowband pump eliminates all of the cross-peaks. Switching between narrowband and broadband pump pulses is straightforward with a pulse shaper.

Untested Ideas for Future Directions. In this section we present a collection of ideas that have not been experimentally tested but could enhance the utility of the technique.

Eq. **9** is only true for systems where the transition dipole undergoes monoexponential rotational diffusion. It does not calculate the correct angle for multiexponential diffusion processes or nondiffusive orientational dynamics, such as angular hydrogen bond jumps (58). Ideally, $\theta_2(t_2)$ could be determined from the raw data without assuming an orientational relaxation model. Here we propose a method to determine $\theta_2(t_2)$ without assuming a model and compare it to $\theta_2(t_2)$ calculated using Eq. **9** and the experimentally obtained D.

Eq. **9** can be rewritten without assuming a relaxation model:

$$\theta_2 = \tan^{-1}\left(\sqrt{\frac{\langle X_iX_iX_iX_i\rangle}{\langle X_iX_iY_iY_i\rangle}}\right). \quad [10]$$

Eq. **10** shows that $\theta_2(t)$ can be calculated if the ratio between the orientational correlation function for XXXX and XXYY is known for all pump-probe delays. Assuming rotational and vibrational motions are uncoupled, the excited state dynamics can be represented as the product of orientational and population kinetics. The population kinetics are unaffected by polarization. Thus, the ratio between diagonal peak signal collected in XXXX and XXYY should depend only on rotations because population dynamics cancel:

$$\frac{S_{X_iX_iX_iX_i}(t)}{S_{X_iX_iY_iY_i}(t)} \propto \frac{\langle X_iX_iX_iX_i\rangle \prod_i e^{-\frac{t}{\tau_i}}}{\langle X_iX_iY_iY_i\rangle \prod_i e^{-\frac{t}{\tau_i}}} = \frac{\langle X_iX_iX_iX_i\rangle}{\langle X_iX_iY_iY_i\rangle}. \quad [11]$$

In Eq. **11**, S_{XXXX} and S_{XXYY} represent the diagonal peak signal from XXXX and XXYY polarizations. τ_i is the time constant for different population relaxation processes. Inserting Eq. **11** into Eq. **10** gives you $\theta_2(t_2)$ as a function of experimental data:

$$\theta_2(t_2) = \tan^{-1}\left(\sqrt{\frac{S_{X_iX_iX_iX_i}(t_2)}{S_{X_iX_iY_iY_i}(t_2)}}\right). \quad [12]$$

The kinetics of the diagonal peak in XXXX and XXYY can be obtained directly from a 2D experiment or a narrowband TA experiment. Fig. 6*B* compares the $\theta_2(t_2)$ calculated using Eq. **9** (red) and $\theta_2(t_2)$ calculated using Eq. **12** (blue). The blue and red curves in Fig. 6*B* are calculated from the same diagonal peak at (2,002, 1,986) cm^{-1}. The two curves differ slightly because the red curve is obtained from a model and the blue curve is obtained directly from data. $\theta_2(t_2)$ calculated using Eqs. **9** and **12** are in qualitative agreement, verifying that this method performs well for IDC in this study. Note that, as expected, $\theta_2(t_2)$ starts near 60° at $t_2 = 0$ and asymptotically approaches 45° with increasing pump-probe delay.

This analysis verifies that model independent method proposed above works for the case of monoexponential orientational relaxation dynamics. We posit that it will also calculate the correct compensation angles for multiexponential and nondiffusive relaxation dynamics as well. This method could work well where one ensemble of oscillators undergoes anisotropy decay on multiple timescales. An example of this phenomenon is the multiexponential rotational dynamics predicted by the wobbling-in-a-cone model (59).

The case in which there are multiple ensembles with different orientational relaxation dynamics is more complicated. Multiple ensembles could result in two or more diagonal peaks, each with its own anisotropy decays. If the ensembles have the same frequency or overlapping spectra, then there would be a single diagonal peak with multiple anisotropy decay timescales. This situation could be caused by two different molecules in solution, or two functional groups with uncorrelated rotations.

In the case of spectrally resolved peaks with different orientational dynamics, only one peak can be eliminated at a time, and each peak will require a different $\theta_2(t_2)$. If diagonal peaks from multiple ensembles spectrally overlap, then the compensation angle can be set to destructively interfere the signals using Eq. **12**. If the overlapping spectra have the same off-diagonal anharmonicities, then both the fundamental and overtone peaks would interfere. Otherwise, only the fundamental will be eliminated. It might be interesting to see if $<0°,0°,+\theta_2(t_2),-\theta_2(t_2)>$ could be varied to deconvolute overlapping spectra. The simplest case would be if the orientational dynamics of each peak are known a priori, then the angles $\theta_2(t_2)$ could be set to preferentially eliminate one peak over the other, deconvoluting the overlapping spectra.

Spectral inhomogeneity and spectral diffusion would also influence the spectra. An inhomogeneous distribution is analogous to multiple ensembles distributed along the linewidth of the absorption spectrum. If a single angle does not remove a diagonal peak in its entirety, then there must be multiple rotational diffusion times along the diagonal, such as has been observed in the OH stretch of water (60). Spectral diffusion will appear as an increase in the antidiagonal linewidth if it changes the transition dipole direction. If spectral diffusion does not accompany rotational diffusion or energy transfer to nonparallel modes, then it will not be observed for $<0°,0°,+\theta_2(t_2),-\theta_2(t_2)>$. Thus, this polarization scheme might be useful for observing spectral diffusion dynamics that are correlated orientational decay, such as angular hydrogen bond jumps (58).

Demonstrations here have focused on 3D isotropic conditions. This method should also work for 2D isotropic conditions as well. The orientational correlation functions including rotations under 2D isotropic conditions have been reported before (37). By repeating derivations in *Theory* using the equations in ref. 37, the compensation angles for 2D isotropic conditions can be derived.

Finally, we note that as one increases $<0°,0°,+\theta,-\theta>$ from 45° to 90° the diagonal peaks change sign, but the cross-peaks do not (when calculating ΔOD). In 2D spectroscopy, instead of completely eliminating the diagonal peaks that fact might be used to destructively interfere a residual portion of the diagonal peaks with the on-diagonal cross-peaks, thereby further reducing features along the diagonal. In TA spectroscopy, one might destructively interfere cross-peak features with the bleach, effectively generating a difference spectrum.

Conclusions

We identify and demonstrate an overlooked polarization scheme that expands the capabilities of pump-probe geometry spectroscopies, like pulse-shaping 2D and TA spectroscopies. By adding two polarizers to a TA or 2D spectrometer, one can eliminate diagonal peaks and expose cross-peaks created by couplings. For 2D spectroscopy, weak cross-peaks near the diagonal can be observed. For TA spectroscopy, cross-peaks that directly report on coupling can now be measured. Previously, cross-peak measurements were the domain of 2D spectroscopy. Now with $<0°,0°,+60°,-60°>$, TA spectroscopy can provide much of the same information as 2D spectroscopy.

Using $<0°,0°,+60°,-60°>$, diagonal peaks reappear at later pump-probe delays, caused exclusively by orientational relaxation. Diagonal peaks can be eliminated at later delays by adjusting the polarization as a function of pump-probe delay, i.e., $<0°,0°,+\theta_2(t_2),-\theta_2(t_2)>$. The compensation angle, $\theta_2(t_2)$, can be

calculated from the rotational diffusion coefficient. Alternatively, the orientational dynamics can be studied by measuring the reappearance of peaks.

We also suggested a number of aspirational ideas that are not tested but may prove useful once they are developed, such as using $<0°,0°,+\theta_2(t_2),-\theta_2(t_2)>$ to probe orientational relaxation, deconvolute spectra, and identify complex rotational motions. Although our demonstrations were performed in the mid-IR, the technique applies to all third-order spectroscopies studying 3D isotropic systems. We intend to apply the technique to kinetically evolving processes like amyloid aggregation and anticipate useful applications in biological light-harvesting proteins and photovoltaic materials, among other applications.

Materials and Methods

Our 2D IR spectrometer is very similar to a traditional TA spectrometer, with the addition of a pulse shaper in the pump beam (61). The 1,032-nm, 150-μJ, and 270-fs output of a 100-kHz Yb:KGW regenerative amplifier (Pharos; Light Conversion) was directed into a two-stage, home-built optical parametric amplifier and difference frequency generation stage, both of which have been described in detail elsewhere (42). The home-built setup generated 0.4-μJ pulses at 4.9 μm. The mid-IR beam was split along a pump and probe path using a 90:10 CaF_2 beam splitter. The probe was directed into a motorized delay stage to control the waiting time between the probe and pump pulses. The pump beam is directed into a horizontal mid-IR pulse shaper based on a germanium acousto-optic modulator (AOM), similar to that used by Phasetech Spectroscopy, Inc. The t_1 delay was measured out to a final delay of 4 ps. For most measurements, a 6-μs mask was used, filling roughly half the aperture of the AOM. Bandwidth loss due to angular dispersion in the shaper was mitigated using active Bragg angle compensation (62). Final pump bandwidth at full width at half maximum was 100 cm^{-1}. The probe bandwidth was 115 cm^{-1}.

The pump pulse pair (E_1 and E_2) and the probe pulse (E_3) are focused using 90° off-axis parabolic mirrors. After overlap at the sample, the probe and signal fields were detected using a 1 × 64 element mercury cadmium telluride (MCT) array (Infrared Systems). Analog-to-digital conversion of the MCT signal was performed using 100-kHz mid-IR detection electronics (Jackhammer; Phasetech Spectroscopy) (42).

Polarization of the pump and probe fields were coarsely adjusted using (λ/2) waveplates placed in the pump and probe paths before the first parabolic mirror. The polarization of the pulses needs to be accurate to within 1°, so wire-grid polarizers were placed between the first parabolic mirror and the sample. A third wire-grid polarizer is placed between the sample and the second parabolic mirror to adjust the projection of emitted fields onto a common axis (i.e., the E_{emit} polarization). This optical layout is shown clearly in *SI Appendix*, Fig. S1.

Eye lens samples were obtained postmortem from the Lion's Eye Bank of Wisconsin. All identifying information was removed. The Minimal Risk Institutional Review Board (Health Sciences) at the University of Wisconsin–Madison determined this study was exempt from obtaining informed consent. Sample preparation details are reported elsewhere (50).

Data Availability. Analysis codes and raw data have been deposited in Figshare (DOIs: https://doi.org/10.6084/m9.figshare.16945618.v1, https://doi.org/10.6084/m9.figshare.16945636.v1, https://doi.org/10.6084/m9.figshare.16945657.v1, https://doi.org/10.6084/m9.figshare.16945675.v1, https://doi.org/10.6084/m9.figshare.16945684.v1, and https://doi.org/10.6084/m9.figshare.16945702.v1) (63–68).

ACKNOWLEDGMENTS. This work was funded by the NIH under award numbers R01GM102387 and R01DK079895. Support for this research was provided by the Office of the Vice Chancellor for Research and Graduate Education at the University of Wisconsin–Madison with funding from the Wisconsin Alumni Research Foundation. Eye lens samples were provided by the Lion's Eye Bank of Wisconsin. We acknowledge Ariel Alperstein for help with eye lenses. K.M.F. is grateful for funding from the NSF Graduate Research Fellowship Program under grant DGE-1747503. Any opinions, findings, and conclusions or recommendations expressed in this material are those of the authors and do not necessarily reflect the views of the NSF.

1. R. R. Birss, "Spatial symmetry" in *Symmetry and Magnetism*, E. P. Wohlfarth, Ed. (North Holland Publishing Co., 1964), pp. 18–73.
2. H. E. Lessing, A. von Jena, M. Reichert, Orientational aspect of transient absorption in solutions. *Chem. Phys. Lett.* **36**, 517–522 (1975).
3. A. B. Meyers, R. M. Hochstrasser, Comparison of four-wave mixing techniques for studying orientational relaxation. *IEEE J. Quantum Electron.* **22**, 1482–1492 (1986).
4. R. M. Hochstrasser, Two-dimensional IR-spectroscopy: Polarization anisotropy effects. *J. Chem. Phys.* **266**, 273–284 (2001).
5. P. Hamm, M. Zanni, *Concepts and Methods of 2D Infrared Spectroscopy* (Cambridge University Press, 2011).
6. G. R. Fleming, J. M. Morris, G. W. Robinson, Direct observation of rotational diffusion by picosecond spectroscopy. *J. Chem. Phys.* **17**, 91–100 (1976).
7. H. E. Lessing, A. von Jena, Separation of rotational diffusion and level kinetics in transient absorption spectroscopy. *Chem. Phys. Lett.* **42**, 213–217 (1976).
8. G. R. Fleming, *Chemical Applications of Ultrafast Spectroscopy* (Oxford University Press, 1986).
9. H. Graener, G. Seifert, A. Laubereau, Direct observation of rotational relaxation times by time-resolved infrared spectroscopy. *Chem. Phys. Lett.* **172**, 435–439 (1990).
10. A. Tokmakoff, Orientational correlation functions and polarization selectivity for nonlinear spectroscopy of isotropic media. I. Third order. *J. Chem. Phys.* **105**, 1–12 (1996).
11. H. S. Tan, I. R. Piletic, M. D. Fayer, Polarization selective spectroscopy experiments: Methodology and pitfalls. *J. Opt. Soc. Am. B* **22**, 2009–2017 (2009).
12. S. Mukamel, *Principles of Nonlinear Optical Spectroscopy* (Oxford University Press, 1995).
13. M. Cho, *Two-Dimensional Optical Spectroscopy* (Taylor & Francis Group, LLC, 2009).
14. M. C. Asplund, M. T. Zanni, R. M. Hochstrasser, Two-dimensional infrared spectroscopy of peptides by phase-controlled femtosecond vibrational photon echoes. *Proc. Natl. Acad. Sci. U.S.A.* **97**, 8219–8224 (2000).
15. O. Golonzka, M. Khalil, N. Demirdöven, A. Tokmakoff, Vibrational anharmonicities revealed by coherent two-dimensional infrared spectroscopy. *Phys. Rev. Lett.* **86**, 2154–2157 (2001).
16. J. D. Hybl, A. A. Ferro, D. M. Jonas, Two-dimensional Fourier transform electronic spectroscopy. *J. Chem. Phys.* **115**, 6606–6622 (2001).
17. O. Golonzka, A. Tokmakoff, Polarization-selective third-order spectroscopy of coupled vibronic states. *J. Chem. Phys.* **115**, 297–309 (2001).
18. M. T. Zanni, N. H. Ge, Y. S. Kim, R. M. Hochstrasser, Two-dimensional IR spectroscopy can be designed to eliminate the diagonal peaks and expose only the crosspeaks needed for structure determination. *Proc. Natl. Acad. Sci. U.S.A.* **98**, 11265–11270 (2001).
19. J. A. Myers, K. L. Lewis, P. F. Tekavec, J. P. Ogilvie, Two-color two-dimensional Fourier transform electronic spectroscopy with a pulse-shaper. *Opt. Express* **16**, 17420–17428 (2008).
20. J. Réhault, J. Helbing, Angle determination and scattering suppression in polarization-enhanced two-dimensional infrared spectroscopy in the pump-probe geometry. *Opt. Express* **20**, 21665–21677 (2012).
21. J. Dreyer, A. M. Moran, S. Mukamel, Tensor components in three pulse vibrational echoes of a rigid dipeptide. *Bull. Korean Chem. Soc.* **24**, 1091–1096 (2003).
22. E. L. Read *et al.*, Cross-peak-specific two-dimensional electronic spectroscopy. *Proc. Natl. Acad. Sci. U.S.A.* **104**, 14203–14208 (2007).
23. N. S. Ginsberg *et al.*, Solving structure in the CP29 light harvesting complex with polarization-phased 2D electronic spectroscopy. *Proc. Natl. Acad. Sci. U.S.A.* **108**, 3848–3853 (2011).
24. S. Woutersen, P. Hamm, Structure determination of trialanine in water using polarization sensitive two-dimensional vibrational spectroscopy. *J. Phys. Chem. B* **104**, 11316–11320 (2000).
25. R. Yuan, M. D. Fayer, Dynamics of water molecules and ions in concentrated lithium chloride solutions probed with ultrafast 2D IR spectroscopy. *J. Phys. Chem. B* **123**, 7628–7639 (2019).
26. P. Hamm, M. Lim, W. F. DeGrado, R. M. Hochstrasser, Pump/probe self-heterodyned 2D spectroscopy of vibrational transitions of a small globular peptide. *J. Chem. Phys.* **112**, 1907–1916 (1999).
27. G. Panitchayangkoon *et al.*, Long-lived quantum coherence in photosynthetic complexes at physiological temperature. *Proc. Natl. Acad. Sci. U.S.A.* **107**, 12766–12770 (2010).
28. A. T. Krummel, P. Mukherjee, M. T. Zanni, Inter and intrastrand vibrational coupling in DNA studied with heterodyned 2D-IR spectroscopy. *J. Phys. Chem. B* **107**, 9165–9169 (2003).
29. H. Maekawa, F. Formaggio, C. Toniolo, N. H. Ge, Onset of 310-helical secondary structure in aib oligopeptides probed by coherent 2D IR spectroscopy. *J. Am. Chem. Soc.* **130**, 6556–6566 (2008).
30. N. Sengupta *et al.*, Sensitivity of 2D IR spectra to peptide helicity: A concerted experimental and simulation study of an octapeptide. *J. Phys. Chem. B* **113**, 12037–12049 (2009).
31. S. Westenhoff, D. Paleček, P. Edlund, P. Smith, D. Zigmantas, Coherent picosecond exciton dynamics in a photosynthetic reaction center. *J. Am. Chem. Soc.* **134**, 16484–16487 (2012).
32. G. S. Schlau-Cohen *et al.*, Elucidation of the timescales and origins of quantum electronic coherence in LHCII. *Nat. Chem.* **4**, 389–395 (2012).
33. A. F. Fidler, V. P. Singh, P. D. Long, P. D. Dahlberg, G. S. Engel, Time scales of coherent dynamics in the light-harvesting complex 2 (LH2) of Rhodobacter Sphaeroides. *J. Phys. Chem. Lett.* **4**, 1404–1409 (2013).
34. L. Chuntonov, D. G. Kuroda, A. Ghosh, J. Ma, R. M. Hochstrasser, Quantum beats and coherence decay in degenerate states split by solvation. *J. Phys. Chem. Lett.* **4**, 1866–1871 (2013).

35. G. H. Richards, K. E. Wilk, P. M. G. Curmi, J. A. Davis, Disentangling electronic and vibrational coherence in the Phycocyanin-645 light-harvesting complex. *J. Phys. Chem. Lett.* **5**, 43–49 (2014).
36. H. Maekawa, G. Ballano, F. Formaggio, C. Toniolo, N. H. Ge, 13C=18O/15N isotope dependence of the amide-I/II 2D IR cross peaks for the fully extended peptides. *J. Phys. Chem. C* **118**, 29448–29457 (2014).
37. R. Mehlenbacher *et al.*, Polarization-controlled two-dimensional white-light spectroscopy of semiconducting carbon nanotube thin films. *J. Phys. Chem. C* **120**, 17069–17080 (2016).
38. E. Thyrhaug *et al.*, Identification and characterization of diverse coherences in the Fenna-Matthews-Olson complex. *Nat. Chem.* **10**, 780–786 (2018).
39. S. H. Shim, D. B. Strasfeld, Y. L. Ling, M. T. Zanni, Automated 2D IR spectroscopy using a mid-IR pulse shaper and application of this technology to the human islet amyloid polypeptide. *Proc. Natl. Acad. Sci. U.S.A.* **104**, 14197–14202 (2007).
40. E. M. Grumstrup, S. H. Shim, M. A. Montgomery, N. H. Damrauer, M. T. Zanni, Facile collection of two-dimensional electronic spectra using femtosecond pulse-shaping technology. *Opt. Express* **15**, 16681–16689 (2007).
41. N. M. Kearns, R. D. Mehlenbacher, A. C. Jones, M. T. Zanni, Broadband 2D electronic spectrometer using white light and pulse shaping: Noise and signal evaluation at 1 and 100 kHz. *Opt. Express* **25**, 7869–7883 (2017).
42. K. M. Farrell *et al.*, Shot-to-shot 2D IR spectroscopy at 100 kHz using a Yb laser and custom-designed electronics. *Opt. Express* **28**, 33584–33602 (2020).
43. C. T. Middleton, D. B. Strasfeld, M. T. Zanni, Polarization shaping in the mid-IR and polarization-based balanced heterodyne detection with application to 2D IR spectroscopy. *Opt. Express* **17**, 14526–14533 (2009).
44. J. Helbing, P. Hamm, Compact implementation of Fourier transform two-dimensional IR spectroscopy without phase ambiguity. *J. Opt. Soc. Am. B* **28**, 171–178 (2011).
45. W. Xiong, M. T. Zanni, Signal enhancement and background cancellation in collinear two-dimensional spectroscopies. *Opt. Lett.* **33**, 1371–1373 (2008).
46. H. S. Chung, M. Khalil, A. W. Smith, A. Tokmakoff, Transient two-dimensional IR spectrometer for probing nanosecond temperature-jump kinetics. *Rev. Sci. Instrum.* **78**, 063101 (2007).
47. J. Réhault, M. Maiuri, A. Oriana, G. Cerullo, Two-dimensional electronic spectroscopy with birefringent wedges. *Rev. Sci. Instrum.* **85**, 123107 (2014).
48. F. Ding, E. C. Fulmer, M. T. Zanni, Heterodyned fifth-order two-dimensional IR spectroscopy: Third-quantum states and polarization selectivity. *J. Chem. Phys.* **123**, 94502 (2005).
49. M. Khalil, N. Demirdöven, A. Tokmakoff, Vibrational coherence transfer characterized with Fourier-transform 2D IR spectroscopy. *J. Chem. Phys.* **121**, 362–373 (2004).
50. A. M. Alperstein, J. S. Ostrander, T. O. Zhang, M. T. Zanni, Amyloid found in human cataracts with two-dimensional infrared spectroscopy. *Proc. Natl. Acad. Sci. U.S.A.* **116**, 6602–6607 (2019).
51. M. K. Petti *et al.*, A proposed method to obtain surface specificity with pump-probe and 2D spectroscopies. *J. Phys. Chem. A* **124**, 3471–3483 (2020).
52. M. K. Petti *et al.*, Enhancing the signal strength of surface sensitive 2D IR spectroscopy. *J. Chem. Phys.* **150**, 024707 (2019).
53. J. Nishida, C. Yan, M. D. Fayer, Enhanced nonlinear spectroscopy for monolayers and thin films in near-Brewster's angle reflection pump-probe geometry. *J. Chem. Phys.* **146**, 094201 (2017).
54. B. Berne, R. Pecora, *Dynamic Light Scattering* (Dover Publishing Co., 2000).
55. M. Khalil, N. Demirdöven, A. Tokmakoff, Obtaining absorptive line shapes in two-dimensional infrared vibrational correlation spectra. *Phys. Rev. Lett.* **90**, 047401 (2003).
56. S. Woutersen, H. J. Bakker, Resonant intermolecular energy transfer in liquid water. *Nature* **402**, 507–509 (1999).
57. I. G. Scheblykin, A. Yartsev, T. Pullerits, V. Gulbinas, V. Sundström, Excited state and charge photogeneration dynamics in conjugated polymers. *J. Phys. Chem. B* **111**, 6303–6321 (2007).
58. D. Laage, J. T. Hynes, A molecular jump mechanism of water reorientation. *Science* **311**, 832–835 (2006).
59. H. S. Tan, I. R. Piletic, M. D. Fayer, Orientational dynamics of water confined on a nanometer length scale in reverse micelles. *J. Chem. Phys.* **122**, 174501 (2005).
60. D. Laage, G. Stirnemann, F. Sterpone, J. T. Hynes, Water jump reorientation: From theoretical prediction to experimental observation. *Acc. Chem. Res.* **45**, 53–62 (2012).
61. S. H. Shim, M. T. Zanni, How to turn your pump-probe instrument into a multidimensional spectrometer: 2D IR and vis spectroscopies via pulse shaping. *Phys. Chem. Chem. Phys.* **11**, 748–761 (2009).
62. J. M. Nite, J. D. Cyran, A. T. Krummel, Active Bragg angle compensation for shaping ultrafast mid-infrared pulses. *Opt. Express* **20**, 23912–23920 (2012).
63. K. Farrell, N. Yang, M. Zanni, Analysis and simulation codes for "A polarization scheme that resolves cross peaks with transient absorption and eliminates peaks in 2D spectroscopy." Figshare. https://doi.org/10.6084/m9.figshare.16945618.v1 (Deposited 11 September 2021).
64. K. Farrell, N. Yang, M. Zanni, Raw Data for Fig. 1,5, and S5. Figshare. https://doi.org/10.6084/m9.figshare.16945636.v1 (Deposited 11 September 2021).
65. K. Farrell, N. Yang, M. Zanni, Raw data for Fig. 2. Figshare.https://doi.org/10.6084/m9.figshare.16945657.v1 (Deposited 11 September 2021).
66. K. Farrell, N. Yang, M. Zanni, Raw Data for Fig. 3. Figshare. https://doi.org/10.6084/m9.figshare.16945675.v1 (Deposited 11 September 2021).
67. K. Farrell, N. Yang, M. Zanni, Raw Data for Fig. 6. Figshare.https://doi.org/10.6084/m9.figshare.16945684.v1 (Deposited 11 September 2021).
68. K. Farrell, N. Yang, M. Zanni, Raw Data for Fig. S6 and S7. Figshare. https://doi.org/10.6084/m9.figshare.16945702.v1 (Deposited 11 September 2021).